Letter

Competition of density waves and superconductivity in twisted tungsten diselenide

Lennart Klebl,[1] Ammon Fischer,[1] Laura Classen,[2] Michael M. Scherer,[3] and Dante M. Kennes[1,4]

[1]*Institut für Theorie der Statistischen Physik, RWTH Aachen University and JARA-Fundamentals of Future Information Technology, D-52056 Aachen, Germany*

[2]*Max Planck Institute for Solid State Research, D-70569 Stuttgart, Germany*

[3]*Institut für Theoretische Physik III, Ruhr-Universität Bochum, D-44801 Bochum, Germany*

[4]*Max Planck Institute for the Structure and Dynamics of Matter, Center for Free Electron Laser Science, D-22761 Hamburg, Germany*

(Received 4 April 2022; accepted 27 February 2023; published 10 March 2023)

Evidence for correlated insulating and superconducting phases around regions of high density of states was reported in the strongly spin-orbit coupled van der Waals material twisted tungsten diselenide ($tWSe_2$). We investigate their origin and interplay by using a functional renormalization group approach that allows one to describe superconducting and spin/charge instabilities in an unbiased way. We map out the phase diagram as a function of filling and perpendicular electric field, and find that the moiré Hubbard model for $tWSe_2$ features mixed-parity superconducting order parameters with s/f-wave and topological d/p-wave symmetry next to (incommensurate) density-wave states. Our work systematically characterizes competing interaction-driven phases in $tWSe_2$ beyond mean-field approximations and provides guidance for experimental measurements by outlining the fingerprint of correlated states in interacting susceptibilities.

DOI: 10.1103/PhysRevResearch.5.L012034

Introduction. The unique control over band structure and interaction parameters in layered van der Waals material stacks with long-range moiré potentials provides an ideal platform to simulate many-body phenomena, and thus holds the promise to advance our understanding of correlated states of matter [1]. Indeed, a plethora of correlated phases were reported in different moiré materials, ranging, e.g., from superconductivity and correlated insulators in twisted multilayer graphene [2–34] and transition metal dichalcogenides (TMDs) [35–38] over excitonic physics [39–41] and generalized Wigner crystals [42] to quantum anomalous Hall states [43].

An example that stands out for its control over a large parameter space is the twisted homobilayer TMD tungsten diselenide ($tWSe_2$), where a correlated insulator occurs for a broad range of twist angles ($\theta \approx 4^\circ \ldots 5.1^\circ$) as a function of carrier density and interlayer displacement field [35,36]. Theoretically, the twist angle and displacement field affect the relative interaction and kinetic energy scales, but also the location and strength of singularities in the density of states (van Hove singularities), and it was pointed out that there is a correspondence between regions of large density of states and insulating behavior. The additional observation of zero resistance states [35] in its immediate vicinity stimulated a debate about possible superconductivity and the underlying mechanisms [44,45].

An unbiased investigation of the electronic phases of $tWSe_2$ has so far remained elusive. In this Letter, we provide such an analysis of the spin-orbit coupled triangular moiré Hubbard model for $tWSe_2$ in the weak to intermediate coupling regime—relevant for experimentally accessible twist angle regimes [46]—using functional renormalization group (FRG) techniques. Within the FRG, all electronic instabilities are treated on equal footing, providing us with a tool that can resolve the competition of various electronic correlations. In particular, the FRG can reveal unconventional mechanisms for superconductivity from repulsive interactions in an unbiased manner for the full *ab initio* inspired and material-specific $tWSe_2$ model. Thereby it substantially goes beyond previous Hartree-Fock studies [46] and parquet renormalization group approaches [44].

We perform large-scale simulations of the doping and displacement-field parameter space and find instabilities towards a variety of density waves around fillings that correspond to Van Hove singularities, which are flanked by pairing instabilities. The wave vectors of the density waves are generally incommensurate and evolve with the displacement field as they follow the nesting vectors of the Fermi surface, which is in line with a previous Hartree-Fock study concentrating on commensurate cases [46]. We find that fluctuations of the density waves mediate attraction in pairing channels of mixed parity in wide parameter regimes and predict the corresponding superconductivity (SC) order to be either of mixed s/f-wave character for strong doping or of mixed d/p-wave character for moderate doping with a preference to form topological $d + id/p + ip$ combinations in the ground state.

Model. The moiré band structure of twisted bilayer WSe_2 in a finite out-of-plane electrical field features a pair of

narrow, isolated, and spin-split bands close to the Fermi level. They are formed by states near valley K or K' of the top and bottom layers of WSe_2, which possess opposite spin orientation due to strong spin-orbit coupling and effective spin-valley locking. As a result, SU(2) spin symmetry is broken, and the moiré band structure reacts strongly to the potential difference between the layers from a displacement field. This can be effectively captured by the moiré Hubbard model [46–49]

$$H = -2t\sum_{\boldsymbol{k},m,\sigma}\cos(\boldsymbol{k}\cdot\boldsymbol{a}_m+\sigma\varphi)c^{\dagger}_{\boldsymbol{k},\sigma}c_{\boldsymbol{k},\sigma}+U\sum_i n_{i,\uparrow}n_{i,\downarrow}, \quad (1)$$

on the triangular moiré lattice with 120° nearest-neighbor vectors $\boldsymbol{a}_{m=1,2,3}$, describing moiré-band electrons $c^{(\dagger)}_{\boldsymbol{k},\sigma}$ with wave vectors $\boldsymbol{k}$ and spin projection $\sigma \in \{\uparrow,\downarrow\}$. Due to spin-valley locking, σ not only describes the spin, but also the valley degree of freedom. The effect of the displacement field is modeled via a spin-dependent nearest-neighbor hopping $te^{i\sigma\varphi}$ with absolute value t and phase φ. Note that the inversion symmetry from the moiré lattice leads to an emergent spin-rotational symmetry at zero displacement field $\varphi = 0$, despite the strong spin-orbit coupling of the individual WSe_2 layers [46]. Moreover, *ab-initio* data show that $\varphi \in [0, \pi/3]$ resembles realistic values of displacement field D [35]. Moreover, *ab initio* data [35] and atomistic tight-binding simulations [see Supplemental Material (SM) [50]] show that $\varphi \in [0, \pi/3]$ resembles realistic values of displacement field D, and that $\varphi \tilde{\propto} D$. The Hubbard interaction U dominates the Coulomb interaction [48] and nonlocal short-ranged interactions can be screened via substrate engineering [51].

Method. To study competing phases in this triangular lattice moiré Hubbard model, we employ the FRG and identify the leading Fermi-surface instabilities including different types of density-wave and superconducting instabilities on equal footing. We use an approximation which exclusively focuses on the FRG flow of the spin-dependent two-particle interaction vertex $\Gamma^{(4)}$. Technically, the FRG introduces a scale parameter Λ to interpolate smoothly from the free theory at $\Lambda = \infty$ to the interacting one at $\Lambda = 0$. Ordering tendencies are indicated by a divergence of $\Gamma^{(4)}$ at finite $\Lambda = \Lambda_c$, where, with our choice of regulator, Λ_c corresponds to the onset temperature of strong correlations. Using the effective vertex at the critical scale Λ_c we can classify the ordering tendencies straightforwardly either as spin/charge density waves (DWs) or as superconductors. For the present system, we have extended the standard correlated-electron FRG scheme [52]: (1) the Hamiltonian in Eq. (1) does not possess an SU(2)-spin invariance and we have adapted the FRG equations accordingly, and (2) instead of the widespread scheme of discretizing only wave vectors on the Fermi surface, we have employed a scheme in which we finely resolve the full Brillouin zone (BZ). This facilitates to also resolve incommensurate density-wave ordering. We note that the latter extension requires a highly efficient numerical implementation to be able to handle the $\sim 3.06 \times 10^9$ coupled ordinary differential equations for the interaction vertex. For details of the FRG implementation and the analysis of phases, see [50].

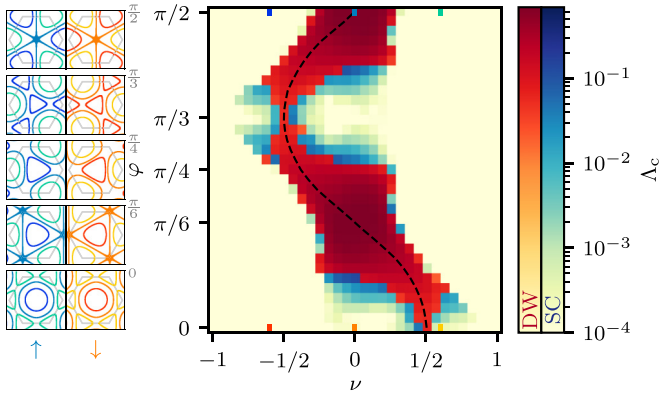

FIG. 1. FRG phase diagram of moiré-Hubbard model for $tWSe_2$. We plot the critical scale Λ_c of the FRG flow that corresponds to an onset temperature of the corresponding correlations and vary the filling factor ν and effective displacement field φ. The panels on the left display Fermi surfaces for $\varphi \in \{0, \pi/6, \pi/4, \pi/3, \pi/2\}$ (bottom to top), both spin polarizations (left: $\sigma =\uparrow$; right: $\sigma =\downarrow$), and three values of $\nu \in \{-0.6, 0, 0.6\}$. The employed FRG approach resolves whether the system tends to order in a spin/density-wave (DW) or superconducting (SC) state, which is encoded as color. Blue regions correspond to SC phases with high Λ_c and red regions correspond to DW phases with high Λ_c. Yellow regions show no ordering tendency within our approximations and thus are predicted to remain metallic. The center of the DW region corresponds to the position of the Van Hove singularity for each φ, indicated by the dashed black line. SC phases emerge upon doping slightly away from the DW states.

Phase diagram. Figure 1 summarizes the main results at intermediate interaction strength $U = 6t \lesssim 0.7W$ (with the bandwidth W) as a function of the filling ν and field-dependent phase φ. Here $\nu = -1$ corresponds to completely empty, $\nu = 0$ to half-filled, and $\nu = 1$ to completely filled moiré bands. We adjust the filling by adding a chemical potential term to the Hamiltonian and the given values refer to the filling fraction of the single-particle dispersion. Upon varying φ, the DW instabilities follow the location of the Van Hove singularity (VHS). The DW region is most extended around $\varphi = \pi/6$ and $\nu = 0$, where the system has a higher-order VHS [46,53]. Given the significant enhancement of density of states at the higher-order VHS as well as the nesting property of the Fermi surface, the DW instability there occurs at high critical scale and in an extended filling region. At the borders of the DW region, SC order emerges. The size of the SC regions strongly varies with ν and φ. Remarkably, for the $\nu = 0$ vertical line, i.e., at half filling, we predict SC order for a substantial fraction of values of φ, interrupted by similarly dominant DW regions. Our findings support the intuitive picture that unconventional SC is driven by the strong spin and charge fluctuations close to the DW instabilities, which we can clearly see in the evolution of the vertex as a function of the renormalization group scale (see SM [50]).

Density-wave states. The strong effect of the displacement field on the band structure also leads to a changing Fermi surface with varying φ. In turn, the singular scattering processes of the DW instabilities correspond to modified wave-vector transfers. To resolve this evolution in detail, we characterize the momentum and spin structure of the DW

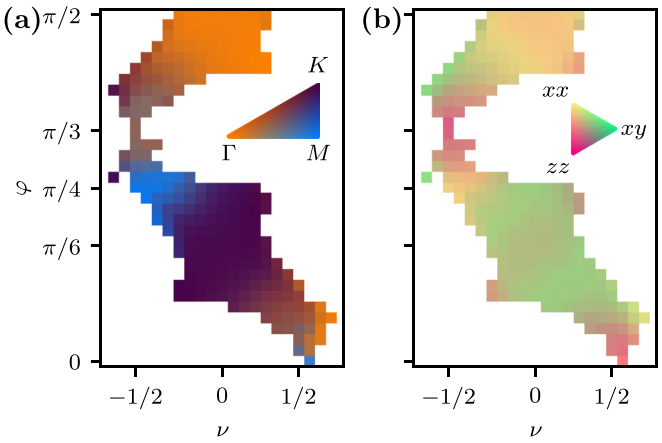

FIG. 2. Momentum and spin structure of spin/density-wave phases. (a) Dominant transfer momentum $\bar{\boldsymbol{q}}$ of particle-hole susceptibility color-coded for all DW instabilities in the phase diagram. There are pronounced regions of commensurate ordering vectors: Γ at $\varphi = \pi/2$ (orange), K at $\varphi = \pi/6$ (dark purple), and M at $\varphi = \pi/4$ (blue). The connecting regions in between show incommensurate ordering vectors. Note the SU(2) symmetric point $\varphi = 0$ where M is the dominant ordering vector. (b) Spin structure of particle-hole susceptibility. The relative weight of the χ^{xx} (yellow), χ^{xy} (green), and χ^{zz} (pink) components is shown for the same DW instabilities as in (a). All other nonzero spin components of the physical susceptibility are symmetry equivalent to either χ^{xx}, χ^{xy}, or χ^{zz}—spin rotational symmetry around the z axis implies $\chi^{xx} = \chi^{yy}$ and $\chi^{xy} \propto \chi^{yx}$. For zero electric field (i.e., $\varphi = 0$), the system is isotropic in spin space thus showing perfect degeneracy of the xx (yy) and zz components. Upon increasing φ, the zz component is strengthened and then giving way to a large region of xy-plane (xx, xy) ordering. At $\varphi = \pi/4$, the xy (yx) component is weakened and for slightly larger φ giving rise to zz ordering. For $\varphi = \pi/2$, the system favors xx (yy) and zz correlations.

states (see Fig. 2), and calculate the particle-hole susceptibilities

$$\chi^{D}_{\sigma_1\ldots\sigma_4}(\boldsymbol{q}) = \quad \sigma_1 \; \sigma_2 \quad \boldsymbol{k}-\boldsymbol{q} \quad \boldsymbol{k}'-\boldsymbol{q} \quad \sigma_3 \; \sigma_4 \quad \boldsymbol{k} \quad \Gamma^{(4),\Lambda_c} \quad \boldsymbol{k}'$$

$$= N_{\boldsymbol{k}}^{-2} \sum_{\sigma_{1'}\sigma_{2'}\sigma_{3'}\sigma_{4'},\boldsymbol{k},\boldsymbol{k}'} \chi^{0,\Lambda_c}_{\sigma_1\sigma_2\sigma_{1'}\sigma_{2'}}(\boldsymbol{q},\boldsymbol{k}) \times \Gamma^{(4),\Lambda_c}_{\sigma_{2'},\sigma_{3'},\sigma_{1'},\sigma_{4'}}(\boldsymbol{k},\boldsymbol{k}'-\boldsymbol{q},\boldsymbol{k}-\boldsymbol{q}) \times \chi^{0,\Lambda_c}_{\sigma_{3'}\sigma_{4'}\sigma_3\sigma_4}(\boldsymbol{q},\boldsymbol{k}'), \tag{2}$$

$$\chi^{ij}(\boldsymbol{q}) = \sum_{\sigma_1\sigma_2\sigma_3\sigma_4} \sigma_i^{\sigma_2\sigma_1} \chi^{D}_{\sigma_1\sigma_2\sigma_3\sigma_4}(\boldsymbol{q}) \sigma_j^{\sigma_3\sigma_4} \tag{3}$$

for all DW-state regions in Fig. 1. Here, $\chi^{D}_{\sigma_1,\ldots,\sigma_4}$ denotes the four-point particle-hole susceptibility and χ^{ij} is its projection to the physical channels $i, j \in \{0, x, y, z\}$, where 0 and x, y, z denote charge and spin, respectively. In Eq. (2), we use the four-point vertex $\Gamma^{(4),\Lambda_c}_{\sigma_1,\ldots,\sigma_4}(\boldsymbol{k}_1,\boldsymbol{k}_2,\boldsymbol{k}_3)$ at the critical scale $\Lambda = \Lambda_c$ and contract with the noninteracting particle-hole susceptibility $\chi^{0,\Lambda}_{\sigma_1\ldots,\sigma_4}(\boldsymbol{q},\boldsymbol{k})$ [50] in order to account for the cross-channel feedback generated during the FRG flow.

To identify the leading ordering vector $\bar{\boldsymbol{q}}$, we sum out the spin indices of the four-point susceptibility and make a weighted average with the momentum transfer vector. We complement the analysis of $\bar{\boldsymbol{q}}$ in Fig. 2(a) with a map of the dominant spin-spin correlations in Fig. 2(b). By symmetry only three inequivalent spin-spin correlations can be nonzero: $\chi^{xx} = \chi^{yy}$, $\chi^{xy} = -\chi^{yx}$, and χ^{zz}. Moreover, we find that density-density correlations are subleading across the phase diagram. Nevertheless, the spin-orbit coupling of the system leads to coupled spin and charge density waves. These DW instabilities describe symmetry breaking in the spin and valley degrees of freedom at the same time owing to spin-valley locking. For further details on the averaging procedures and density-density correlations, see Ref. [50].

We find that for the region close to $\varphi = \pi/2$ the system exhibits a leading ordering vector of $\bar{\boldsymbol{q}} = \Gamma$, suggesting a ferromagnetic ground state. The weight is almost equally distributed in the xx/yy and zz directions. Moving towards smaller φ and following the VHS, the leading transfer momentum continuously transitions to an extended region around $\varphi \approx \pi/3$ where $\bar{\boldsymbol{q}}$ is incommensurate and accompanied by a strong zz component. Lowering φ further to around $\varphi \lesssim \pi/4$, the support for xx/yy correlations is enhanced and the dominant ordering vector is $\bar{\boldsymbol{q}} \sim M$, indicating an instability consistent with the stripe order found in Ref. [46] or with a more complex superposition of the spin DWs with the three nonequivalent M points as wave vectors [54,55]. Approaching the higher-order VHS at $\varphi = \pi/6$ we see a leading momentum of $\bar{\boldsymbol{q}} = K$ and a change towards xy correlations. Notably, for this choice of φ, the wave vector K (as well as K') is a nesting vector connecting the spin-up with the spin-down Fermi surface. These features signal a twofold degenerate instability that supports the spiral 120° order found in Ref. [46]. An analogous signature is visible in the two small regions at minimal doping at $\varphi \sim \pi/4$ and $\varphi \sim 3\pi/8$. Eventually, letting φ go to zero, the ordering vector continuously approaches Γ, except for a very small region around $\varphi = 0$, i.e., the limit of restored spin-SU(2) invariance, where $\bar{\boldsymbol{q}} = M$. The spin-spin correlations display a slightly more continuous transition towards xx/yy and zz order at $\varphi = 0$, consistent with recovered SU(2) symmetry. The feature at $\varphi = 0$ is in agreement with previous results for the spin-SU(2) invariant triangular-lattice Hubbard model [56–59].

Additionally, we observe that the regions in the phase diagram characterized by a leading momentum of Γ, M, or K are connected by extended regions where the leading momentum is incommensurate. While the commensurate regions are in agreement with previous Hartree-Fock studies [46], the unbiased identification of regions with leading incommensurate momentum which can be readily read off from Fig. 2(a) is one of the advantages of our FRG approach featuring high momentum resolution.

Superconductivity. In the vicinity of the DW ordered states, our FRG approach can detect pairing instabilities driven by spin and charge fluctuations in an unbiased way because particle-hole and pairing channels are coupled. The corresponding SC states may be classified by the symmetry of the order parameter. We use a linearized gap equation with the vertex at the critical scale $\Lambda = \Lambda_c$ (and set the temperature to $T = \Lambda_c$) to obtain the pairing gap functions and their respec-

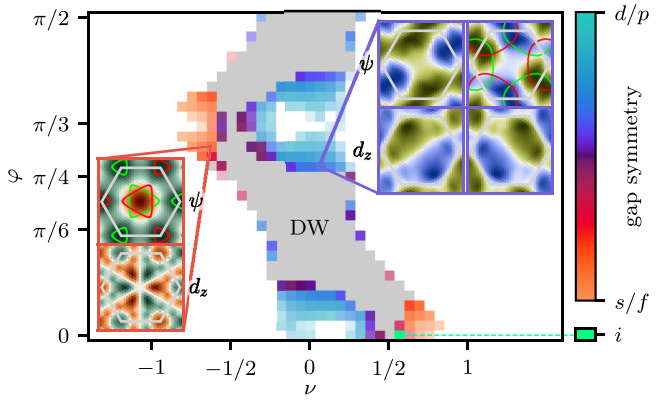

FIG. 3. Properties of the superconducting phases. The regions of superconducting (SC) order are color-coded by their dominant gap symmetry, with cyan standing for d/p-wave SC and orange for (extended) s/f-wave SC. Lower values of Λ_c are indicated by increasing transparency. We plot the logarithmic ratio of s/f-wave and d/p-wave eigenvalues of the linearized gap equation as a continuous color bar to highlight regions of strong competition (purple). The small area of bright green denotes i-wave SC. In the gray region, FRG predicts spin/density-wave order. As for most parts of the phase diagram the system is not SU(2) symmetric; singlet (ψ) and triplet (d_z) amplitudes are intrinsically coupled. For remote regions of filling, the system prefers extended s-wave gaps in the singlet channel and f-wave gaps in the triplet channel (left inset). For fillings closer to zero, two degenerate solutions with d-wave symmetry in the ψ component and p-wave symmetry in the d_z component are found (right inset, two degenerate solutions).

tive amplitudes. As for $\varphi \neq 0$ the system does not obey SU(2) symmetry, we transform the gap $\Delta_{\sigma\sigma'}(\boldsymbol{k})$ to its singlet $[\psi(\boldsymbol{k})]$ and triplet $[\boldsymbol{d}(\boldsymbol{k})]$ components [60]. These are inherently coupled giving rise to mixed-parity (singlet and triplet) SC order. Spin rotational symmetry around the z axis mandates that $d_x = d_y = 0$ for coupled singlet/triplet instabilities.

Additionally, for mixed-parity superconductivity, the singlet and triplet components may describe pairing of different length scales, such that, e.g., an extended s wave (s') in ψ can be combined with an extended f wave (f') in d_z (as long as the two transform in the same representation). Therefore, we distinguish the mixed-parity SC states by their irreducible representations of the C_{3v} symmetry group. We find that the SC phase diagram (cf. Fig. 3) is mostly governed by instabilities transforming in the A_1 or E representations, which we label as s/f and d/p wave, respectively [61]. To resolve the competition between superconducting instabilities, we plot the logarithm of the ratio of d/p-wave and s/f-wave amplitudes that the linearized gap equation provides as a continuous color map. The two insets show examples of d/p-wave symmetric (right inset) and s/f-wave symmetric gap functions in the singlet-triplet basis. The spin-resolved gap functions on the Fermi surfaces are shown in the Supplemental Material [50]. For all instabilities with a dominant (twofold degenerate) d/p-wave instability, the free energy in a subsequent mean-field decoupling is minimized by a chiral $(d+id)/(p+ip)$-wave superposition of order parameters as it allows for a fully gapped Fermi surface. In the SU(2) symmetric case, an i-wave symmetric gap function is supported in a narrow filling window close to the VHS [58] highlighted with green in Fig. 3.

Interestingly, for most parts of the phase diagram in Fig. 3, large filling values of $|\nu| \gtrsim 1/2$ support s/f-wave SC, whereas for small values $|\nu| \lesssim 1/2$, d/p-wave SC is favored. The DW phases in Fig. 2, on the other hand, have no clear dependence solely on ν. For example, there are points of dominant in-plane spiral order at $\nu \approx -1/2$ and $\varphi \approx 3\pi/8$ as well as at $\nu \approx 0$ and $\varphi \approx \pi/4$ [purple in Fig. 2(a) and green in Fig. 2(b)]. The adjacent superconducting domes are of manifestly different pairing symmetry, e.g., s/f wave in the former and d/p wave in the latter case (cf. Fig. 3). These observations shed light on the mechanism responsible for the type of SC order: The data suggest that the precise spin and momentum structure of the dominant spin/charge fluctuations is *irrelevant* as long as it is present and instead, the topology of the Fermi surfaces is responsible for the different symmetries of SC order parameter found, e.g., small pockets around K, K' vs large closed lines around Γ. The extended nature of the superconducting instabilities (p/d wave: nearest neighbors; s/f wave: next-nearest neighbors) indicates that DW fluctuations with $\boldsymbol{q} \neq 0$ represent the pairing glue. This statement is supported by the observation that for $\varphi \lesssim \pi/2$, the DW transfer momentum is intra-VHS, i.e., $\bar{\boldsymbol{q}} = \Gamma$, and SC is suppressed. Finally, we note that at $\varphi = \pi/3$ an additional peak at $\boldsymbol{q} = K^{(\prime)}$ appears in the pairing susceptibility, indicative of enhanced pair-density-wave correlations, which were also reported recently in Ref. [45].

Discussion. In this work we calculate the two-particle interaction vertex $\Gamma^{(4)}$ within the FRG to study the electronic phase diagram of a spin-orbit coupled moiré Hubbard model on the triangular lattice. In the group of twisted bilayer TMDs, this model is believed to have various experimental realizations through different AA-stacked homobilayer systems. Even more so, recent measurements show that correlated insulating and possible superconducting states are in fact realized in twisted WSe_2 [35,36]. Our work offers an unbiased characterization of competing electronic correlations in twisted WSe_2. As a result of our large-scale simulations, we provide the FRG phase diagram as a function of filling ν and displacement field φ in the intermediate coupling regime ($U = 6t$). We firmly establish a beyond mean-field characterization of intricate density-wave orderings close to the van Hove singularity of the system. Furthermore, the FRG reveals pairing instabilities mediated by spin and charge fluctuations so that the wide variety of DW phases is complemented by a relatively large area of the phase diagram where superconducting correlations dominate. For nonzero displacement field, the SC orderings can be divided into d/p-wave order (including higher harmonics) for weak doping and s/f-wave order for strong doping. While both order parameters are unconventional in nature and caused by spin/charge fluctuations, the s/f wave is nodal and the d/p wave is chiral ($d+id/p+ip$). Thus, we propose spectroscopy experiments on WSe_2 to verify the transition of a nodal to a chiral (fully gapped) SC order. Time-reversal symmetry breaking in the chiral state can also be detected via Kerr rotation [62] or muon spin relaxation [63]. We also note that the interplay with other nearby states can alternatively yield nematic superconductivity [64,65], which can be detected by spatial anisotropies [17,66–68].

In future works, we are aiming towards extending our studies on non-SU(2) and multiorbital moiré systems with

band structures and interactions closely motivated by materials. This includes, but is not limited to, systematic studies of longer range and constrained random phase approximation (cRPA)-dressed interactions as an input to the FRG. Furthermore, band structures may be directly fitted to *ab initio* results [69] or generated with Wannierization, paving the road for high-throughput studies of competing orders in two-dimensional (moiré) materials.

Note added. Recently, Ref. [45] appeared providing similar conclusions where applicable.

Acknowledgments. We thank J. Beyer, J. Cano, J. Hauck, A. Leonhardt, A. Millis, A. Pasupathy, A. Schnyder, T. Schäfer, and J. Zang for useful discussions. We acknowledge funding by the Deutsche Forschungsgemeinschaft (DFG, German Research Foundation) under RTG 1995, within the Priority Program SPP 2244 "2DMP" and under Germany's Excellence Strategy–Cluster of Excellence Matter and Light for Quantum Computing (ML4Q) EXC 2004/1-390534769. We acknowledge computational resources provided by the Max Planck Computing and Data Facility and RWTH Aachen University under Project No. rwth0716. This work was supported by the Max Planck–New York City Center for Nonequilibrium Quantum Phenomena. M.M.S. acknowledges support through the DFG Heisenberg program (Project ID 452976698) and SFB 1238 (Project No. C02, Project ID 277146847).

[1] D. M. Kennes, M. Claassen, L. Xian, A. Georges, A. J. Millis, J. Hone, C. R. Dean, D. N. Basov, A. Pasupathy, and A. Rubio, Moiré heterostructures as a condensed matter quantum simulator, Nat. Phys. **17**, 155 (2021).

[2] Y. Cao, V. Fatemi, S. Fang, K. Watanabe, T. Taniguchi, E. Kaxiras, and P. Jarillo-Herrero, Unconventional superconductivity in magic-angle graphene superlattices, Nature (London) **556**, 43 (2018).

[3] Y. Cao, V. Fatemi, A. Demir, S. Fang, S. L. Tomarken, J. Y. Luo, J. D. Sanchez-Yamagishi, K. Watanabe, T. Taniguchi, E. Kaxiras *et al.*, Correlated insulator behaviour at half-filling in magic-angle graphene superlattices, Nature (London) **556**, 80 (2018).

[4] X. Lu, P. Stepanov, W. Yang, M. Xie, M. A. Aamir, I. Das, C. Urgell, K. Watanabe, T. Taniguchi, G. Zhang *et al.*, Superconductors, orbital magnets and correlated states in magic-angle bilayer graphene, Nature (London) **574**, 653 (2019).

[5] Y. Cao, D. Chowdhury, D. Rodan-Legrain, O. Rubies-Bigordà, K. Watanabe, T. Taniguchi, T. Senthil, and P. Jarillo-Herrero, Strange Metal in Magic-Angle Graphene with near Planckian Dissipation, Phys. Rev. Lett. **124**, 076801 (2020).

[6] H. Polshyn, M. Yankowitz, S. Chen, Y. Zhang, K. Watanabe, T. Taniguchi, C. R. Dean, and A. F. Young, Large linear-in-temperature resistivity in twisted bilayer graphene, Nat. Phys. **15**, 1011 (2019).

[7] M. Yankowitz, S. Chen, H. Polshyn, Y. Zhang, K. Watanabe, T. Taniguchi, D. Graf, A. F. Young, and C. R. Dean, Tuning superconductivity in twisted bilayer graphene, Science **363**, 1059 (2019).

[8] X. Liu, Z. Wang, K. Watanabe, T. Taniguchi, O. Vafek, and J. Li, Tuning electron correlation in magic-angle twisted bilayer graphene using Coulomb screening, Science **371**, 1261 (2021).

[9] P. Stepanov, I. Das, X. Lu, A. Fahimniya, K. Watanabe, T. Taniguchi, F. H. Koppens, J. Lischner, L. Levitov, and D. K. Efetov, Untying the insulating and superconducting orders in magic-angle graphene, Nature (London) **583**, 375 (2020).

[10] H. S. Arora, R. Polski, Y. Zhang, A. Thomson, Y. Choi, H. Kim, Z. Lin, I. Z. Wilson, X. Xu, J.-H. Chu *et al.*, Superconductivity in metallic twisted bilayer graphene stabilized by WSe_2, Nature (London) **583**, 379 (2020).

[11] U. Zondiner, A. Rozen, D. Rodan-Legrain, Y. Cao, R. Queiroz, T. Taniguchi, K. Watanabe, Y. Oreg, F. von Oppen, A. Stern *et al.*, Cascade of phase transitions and Dirac revivals in magic-angle graphene, Nature (London) **582**, 203 (2020).

[12] D. Wong, K. P. Nuckolls, M. Oh, B. Lian, S. J. Yonglong Xie, K. Watanabe, T. Taniguchi, B. A. Bernevig, and A. Yazdani, Cascade of electronic transitions in magic-angle twisted bilayer graphene, Nature (London) **582**, 198 (2020).

[13] Y. Xie, B. Lian, B. Jäck, X. Liu, C.-L. Chiu, K. Watanabe, T. Taniguchi, B. A. Bernevig, and A. Yazdani, Spectroscopic signatures of many-body correlations in magic-angle twisted bilayer graphene, Nature (London) **572**, 101 (2019).

[14] A. Kerelsky, L. J. McGilly, D. M. Kennes, L. Xian, M. Yankowitz, S. Chen, K. Watanabe, T. Taniguchi, J. Hone, C. Dean *et al.*, Maximized electron interactions at the magic angle in twisted bilayer graphene, Nature (London) **572**, 95 (2019).

[15] Y. Jiang, X. Lai, K. Watanabe, T. Taniguchi, K. Haule, J. Mao, and E. Y. Andrei, Charge order and broken rotational symmetry in magic-angle twisted bilayer graphene, Nature (London) **573**, 91 (2019).

[16] Y. Choi, J. Kemmer, Y. Peng, A. Thomson, H. Arora, R. Polski, Y. Zhang, H. Ren, J. Alicea, G. Refael *et al.*, Electronic correlations in twisted bilayer graphene near the magic angle, Nat. Phys. **15**, 1174 (2019).

[17] Y. Cao, D. Rodan-Legrain, J. M. Park, N. F. Q. Yuan, K. Watanabe, T. Taniguchi, R. M. Fernandes, L. Fu, and P. Jarillo-Herrero, Nematicity and competing orders in superconducting magic-angle graphene, Science **372**, 264 (2021).

[18] G. W. Burg, J. Zhu, T. Taniguchi, K. Watanabe, A. H. MacDonald, and E. Tutuc, Correlated Insulating States in Twisted Double Bilayer Graphene, Phys. Rev. Lett. **123**, 197702 (2019).

[19] J. M. Park, Y. Cao, K. Watanabe, T. Taniguchi, and P. Jarillo-Herrero, Tunable strongly coupled superconductivity in magic-angle twisted trilayer graphene, Nature (London) **590**, 249 (2021).

[20] Y. Cao, J. M. Park, K. Watanabe, T. Taniguchi, and P. Jarillo-Herrero, Pauli-limit violation and re-entrant superconductivity in moiré graphene, Nature **595**, 526 (2021).

[21] Z. Hao, A. Zimmerman, P. Ledwith, E. Khalaf, D. H. Najafabadi, K. Watanabe, T. Taniguchi, A. Vishwanath, and P. Kim, Electric field–tunable superconductivity in alternating-twist magic-angle trilayer graphene, Science **371**, 1133 (2021).

[22] H. Kim, Y. Choi, C. Lewandowski, A. Thomson, Y. Zhang, R. Polski, K. Watanabe, T. Taniguchi, J. Alicea, and S. Nadj-Perge, Evidence for unconventional superconductivity in twisted trilayer graphene, Nature **606**, 494 (2022).

[23] X. Liu, Z. Hao, E. Khalaf, J. Y. Lee, Y. Ronen, H. Yoo, D. H. Najafabadi, K. Watanabe, T. Taniguchi, A. Vishwanath *et al.*, Tunable spin-polarized correlated states in twisted double bilayer graphene, Nature (London) **583**, 221 (2020).

[24] C. Shen, Y. Chu, Q. Wu, N. Li, S. Wang, Y. Zhao, J. Tang, J. Liu, J. Tian, K. Watanabe *et al.*, Correlated states in twisted double bilayer graphene, Nat. Phys. **16**, 520 (2020).

[25] Y. Cao, D. Rodan-Legrain, O. Rubies-Bigorda, J. M. Park, K. Watanabe, T. Taniguchi, and P. Jarillo-Herrero, Author correction: Tunable correlated states and spin-polarized phases in twisted bilayer–bilayer graphene, Nature (London) **583**, E27 (2020).

[26] C. Rubio-Verdú, S. Turkel, Y. Song, L. Klebl, R. Samajdar, M. S. Scheurer, J. W. Venderbos, K. Watanabe, T. Taniguchi, H. Ochoa *et al.*, Moiré nematic phase in twisted double bilayer graphene, Nat. Phys. **18**, 196 (2022).

[27] G. Chen, A. L. Sharpe, P. Gallagher, I. T. Rosen, E. J. Fox, L. Jiang, B. Lyu, H. Li, K. Watanabe, T. Taniguchi *et al.*, Signatures of tunable superconductivity in a trilayer graphene moiré superlattice, Nature (London) **572**, 215 (2019).

[28] G. Chen, L. Jiang, S. Wu, B. Lyu, H. Li, B. L. Chittari, K. Watanabe, T. Taniguchi, Z. Shi, J. Jung *et al.*, Evidence of a gate-tunable Mott insulator in a trilayer graphene moiré superlattice, Nat. Phys. **15**, 237 (2019).

[29] G. Chen, A. L. Sharpe, E. J. Fox, Y.-H. Zhang, S. Wang, L. Jiang, B. Lyu, H. Li, K. Watanabe, T. Taniguchi *et al.*, Tunable correlated Chern insulator and ferromagnetism in a moiré superlattice, Nature (London) **579**, 56 (2020).

[30] J. M. Park, Y. Cao, L. Xia, S. Sun, K. Watanabe, T. Taniguchi, and P. Jarillo-Herrero, Magic-angle multilayer graphene: A robust family of moiré superconductors, arXiv:2112.10760.

[31] Y. Zhang, R. Polski, C. Lewandowski, A. Thomson, Y. Peng, Y. Choi, H. Kim, K. Watanabe, T. Taniguchi, J. Alicea, F. Von Oppen, G. Refael, and S. Nadj-Perge, Promotion of superconductivity in magic-angle graphene multilayers, Science **377**, 1538 (2022).

[32] G. W. Burg, E. Khalaf, Y. Wang, K. Watanabe, T. Taniguchi, and E. Tutuc, Emergence of correlations in alternating twist quadrilayer graphene, Nat. Mater. **21**, 884 (2022).

[33] A. Kerelsky, C. Rubio-Verdú, L. Xian, D. M. Kennes, D. Halbertal, N. Finney, L. Song, S. Turkel, L. Wang, K. Watanabe *et al.*, Moiréless correlations in ABCA graphene, Proc. Natl. Acad. Sci. USA **118**, e2017366118 (2021).

[34] X. Liu, N. J. Zhang, K. Watanabe, T. Taniguchi, and J. Li, Isospin order in superconducting magic-angle twisted trilayer graphene, Nat. Phys. **18**, 522 (2022).

[35] L. Wang, E.-M. Shih, A. Ghiotto, L. Xian, D. A. Rhodes, C. Tan, M. Claassen, D. M. Kennes, Y. Bai, B. Kim *et al.*, Correlated electronic phases in twisted bilayer transition metal dichalcogenides, Nat. Mater. **19**, 861 (2020).

[36] A. Ghiotto, E.-M. Shih, G. S. Pereira, D. A. Rhodes, B. Kim, J. Zang, A. J. Millis, K. Watanabe, T. Taniguchi, J. C. Hone *et al.*, Quantum criticality in twisted transition metal dichalcogenides, Nature (London) **597**, 345 (2021).

[37] Y. Tang, L. Li, T. Li, Y. Xu, S. Liu, K. Barmak, K. Watanabe, T. Taniguchi, A. H. MacDonald, J. Shan, and K. F. Mak, Simulation of Hubbard model physics in WSe_2/WS_2 moiré superlattices, Nature (London) **579**, 353 (2020).

[38] C. Jin, Z. Tao, T. Li, Y. Xu, Y. Tang, J. Zhu, S. Liu, K. Watanabe, T. Taniguchi, J. C. Hone *et al.*, Stripe phases in WSe_2/WS_2 moiré superlattices, Nat. Mater. **20**, 940 (2021).

[39] C. Jin, E. C. Regan, A. Yan, M. Iqbal Bakti Utama, D. Wang, S. Zhao, Y. Qin, S. Yang, Z. Zheng, S. Shi *et al.*, Observation of moiré excitons in WSe_2/WS_2 heterostructure superlattices, Nature (London) **567**, 76 (2019).

[40] Z. Wang, D. A. Rhodes, K. Watanabe, T. Taniguchi, J. C. Hone, J. Shan, and K. F. Mak, Evidence of high-temperature exciton condensation in two-dimensional atomic double layers, Nature (London) **574**, 76 (2019).

[41] Y. Shimazaki, I. Schwartz, K. Watanabe, T. Taniguchi, M. Kroner, and A. Imamoğlu, Strongly correlated electrons and hybrid excitons in a moiré heterostructure, Nature (London) **580**, 472 (2020).

[42] E. C. Regan, D. Wang, C. Jin, M. I. Bakti Utama, B. Gao, X. Wei, S. Zhao, W. Zhao, Z. Zhang, K. Yumigeta *et al.*, Mott and generalized Wigner crystal states in WSe_2/WS_2 moiré superlattices, Nature (London) **579**, 359 (2020).

[43] T. Li, S. Jiang, B. Shen, Y. Zhang, L. Li, Z. Tao, T. Devakul, K. Watanabe, T. Taniguchi, L. Fu *et al.*, Quantum anomalous Hall effect from intertwined moiré bands, Nature (London) **600**, 641 (2021).

[44] Y.-T. Hsu, F. Wu, and S. Das Sarma, Spin-valley locked instabilities in moiré transition metal dichalcogenides with conventional and higher-order Van Hove singularities, Phys. Rev. B **104**, 195134 (2021).

[45] Y.-M. Wu, Z. W. Wu, and H. Yao, Pair-density-wave and chiral superconductivity in twisted bilayer transition-metal-dichalcogenides, arXiv:2203.05480 [Phys. Rev. Lett. (to be published)].

[46] J. Zang, J. Wang, J. Cano, and A. J. Millis, Hartree-Fock study of the moiré Hubbard model for twisted bilayer transition metal dichalcogenides, Phys. Rev. B **104**, 075150 (2021).

[47] F. Wu, T. Lovorn, E. Tutuc, I. Martin, and A. H. MacDonald, Topological Insulators in Twisted Transition Metal Dichalcogenide Homobilayers, Phys. Rev. Lett. **122**, 086402 (2019).

[48] H. Pan, F. Wu, and S. Das Sarma, Band topology, Hubbard model, Heisenberg model, and Dzyaloshinskii-Moriya interaction in twisted bilayer WSe_2, Phys. Rev. Res. **2**, 033087 (2020).

[49] D. Kiese, Y. He, C. Hickey, A. Rubio, and D. M. Kennes, TMDs as a platform for spin liquid physics: A strong coupling study of twisted bilayer WSe_2, APL Mater. **10**, 031113 (2022).

[50] See Supplemental Material at http://link.aps.org/supplemental/10.1103/PhysRevResearch.5.L012034 for details on the non-SU(2) FRG calculations, evaluation of the effective vertices at the end of the RG flow and comparison of the non-interacting model to an atomistic tight-binding model.

[51] F. Wu, T. Lovorn, E. Tutuc, and A. H. MacDonald, Hubbard Model Physics in Transition Metal Dichalcogenide Moiré Bands, Phys. Rev. Lett. **121**, 026402 (2018).

[52] W. Metzner, M. Salmhofer, C. Honerkamp, V. Meden, and K. Schönhammer, Functional renormalization group approach to correlated fermion systems, Rev. Mod. Phys. **84**, 299 (2012).

[53] A. Shtyk, G. Goldstein, and C. Chamon, Electrons at the monkey saddle: A multicritical Lifshitz point, Phys. Rev. B **95**, 035137 (2017).

[54] R. Nandkishore, G.-W. Chern, and A. V. Chubukov, Itinerant Half-Metal Spin-Density-Wave State on the Hexagonal Lattice, Phys. Rev. Lett. **108**, 227204 (2012).

[55] I. Martin and C. D. Batista, Itinerant Electron-Driven Chiral Magnetic Ordering and Spontaneous Quantum Hall Effect in Triangular Lattice Models, Phys. Rev. Lett. **101**, 156402 (2008).

[56] C. Honerkamp, Instabilities of interacting electrons on the triangular lattice, Phys. Rev. B **68**, 104510 (2003).

[57] M. M. Scherer, D. M. Kennes, and L. Classen, Chiral superconductivity with enhanced quantized Hall responses in moiré transition metal dichalcogenides, npj Quantum Mater. **7**, 100 (2022).

[58] N. Gneist, L. Classen, and M. M. Scherer, Competing instabilities of the extended Hubbard model on the triangular lattice: Truncated-unity functional renormalization group and application to moiré materials, Phys. Rev. B **106**, 125141 (2022).

[59] A. Wietek, R. Rossi, F. Šimkovic, M. Klett, P. Hansmann, M. Ferrero, E. M. Stoudenmire, T. Schäfer, and A. Georges, Mott Insulating States with Competing Orders in the Triangular Lattice Hubbard Model, Phys. Rev. X **11**, 041013 (2021).

[60] M. Sigrist and K. Ueda, "Phenomenological theory of unconventional superconductivity," Rev. Mod. Phys. **63**, 239 (1991).

[61] Note that the symmetry is enhanced to C_{6v} (equivalent to D_{6h} due to the inherent two-dimensional nature of our model) for $\varphi = 0$, where we find pairing instabilities in the E_2 (d wave, E_{2g}), B_1 (f wave, B_{1u}), and A_2 (i wave, A_{2g}) representations.

[62] A. Kapitulnik, Notes on constraints for the observation of polar Kerr effect in complex materials, Phys. B: Condens. Matter **460**, 151 (2015), special issue on electronic crystals (ECRYS-2014).

[63] Z. L. Mahyari, A. Cannell, C. Gomez, S. Tezok, A. Zelati, E. V. L. de Mello, J.-Q. Yan, D. G. Mandrus, and J. E. Sonier, Zero-field μSR search for a time-reversal-symmetry-breaking mixed pairing state in superconducting $Ba_{1-x}K_xFe_2As_2$, Phys. Rev. B **89**, 020502(R) (2014).

[64] V. Kozii, H. Isobe, J. W. F. Venderbos, and L. Fu, Nematic superconductivity stabilized by density wave fluctuations: Possible application to twisted bilayer graphene, Phys. Rev. B **99**, 144507 (2019).

[65] D. V. Chichinadze, L. Classen, and A. V. Chubukov, Nematic superconductivity in twisted bilayer graphene, Phys. Rev. B **101**, 224513 (2020).

[66] S. Yonezawa, K. Tajiri, S. Nakata, Y. Nagai, Z. Wang, K. Segawa, Y. Ando, and Y. Maeno, Thermodynamic evidence for nematic superconductivity in $Cu_xBi_2Se_3$, Nat. Phys. **13**, 123 (2017).

[67] J. Shen, W.-Y. He, N. F. Q. Yuan, Z. Huang, C.-w. Cho, S. H. Lee, Y. S. Hor, K. T. Law, and R. Lortz, Nematic topological superconducting phase in Nb-doped Bi_2Se_3, npj Quantum Mater. **2**, 59 (2017).

[68] T. Asaba, B. J. Lawson, C. Tinsman, L. Chen, P. Corbae, G. Li, Y. Qiu, Y. S. Hor, L. Fu, and L. Li, Rotational Symmetry Breaking in a Trigonal Superconductor Nb-Doped Bi_2Se_3, Phys. Rev. X **7**, 011009 (2017).

[69] L. Klebl, Q. Xu, A. Fischer, L. Xian, M. Claassen, A. Rubio, and D. M. Kennes, Moiré engineering of spin–orbit coupling in twisted platinum diselenide, Electron. Struct. **4**, 014004 (2022).